JISE

A Simultaneous Numerical Integration Routine for the Fast Calculation of Similar Integrations

Aytac ALPARSLAN [1*] ID

[1*] *Department of Electrical and Electronics Engineering, Faculty of Engineering, Trakya University, Edirne, 22030*

Abstract

In this paper, a fast and simultaneous integration routine tailored for obtaining results of multiple numerical integrations is introduced. In the routine, the same nodes are used when integrating different functions along the same integration path. In the paper it is demonstrated by several examples that if the integrands of interest are similar on the integration path, then using the same nodes decreases the computational costs dramatically. While the method is introduced by updating the popular Gauss-Kronrod quadrature rule, the same steps given in the paper can be applied to any other numerical integration rule.

Keywords: Electromagnetic Line Sources, Gauss-Kronrod Quadrature, Layered Media Green's Functions, Numerical Integration, Simultaneous Integration.

1. Introduction

Numerical integration routines are indispensable tools in modern engineering. They are used in nearly every type of advanced engineering problems to obtain the integration result of a given integrand, especially when there is no closed-form analytical result [1–6]. In some problem types, the integration results of multiple integrands may be needed simultaneously. For instance, when obtaining the power flow generated by an electromagnetic source, all of the components of electric and magnetic fields are needed [7–9]. These quantities are usually obtained by computational electromagnetic methods such as finite element method [10], method of moments [11,12] or method of multipoles [13] where numerical integration routines are employed. The integrands of such integrations are usually similar in shape because the locations of the singularities, branch cuts and branch points are observed at the same locations on the integration plane. As a result of this fact, the distribution of nodes obtained by the adaptive numerical integration methods becomes very similar for all the integrands, if not the same. Using this observation, one can use the same set of nodes for all the integrations simultaneously, which eliminates the necessity of calculating the same functions when building up the integrands.

In this paper, a simultaneous integration routine that can be used to numerically integrate similar integrands is introduced. If the multiple integrands have same types of functions as their constituents and have the same distribution of singularities, branch points and cuts around the integration path, the introduced method decreases the computation costs of integrations dramatically.

The paper is organized as follows. In section 2, the method is described in detail by reminding the important aspects of the popular Gauss-Kronrod quadrature rule and the upgrade introduced in the paper. In section 3, numerical examples are given to demonstrate the efficiency and advantages of the method. In Section 4, the outcomes of the paper are listed.

2. Simultaneous Numerical Integration of Similar Integrands by Gauss-Kronrod Quadrature

One of the most popular numerical integration methods that is frequently used in computational electromagnetics is the Gauss-Kronrod rule, which is an upgraded version of the well-known n-point Gauss quadrature rule defined as follows [14]:

$$\int_a^b f(x)dx \approx G_n = \sum_{i=1}^n w_i f(x_i) = \vec{w} f(\vec{x}) \tag{1}$$

where w_i and x_i are the weights and nodes of the n-point Gauss quadrature rule, which are listed in the row and column vectors $\vec{w}_{(1 \times n)}$ and $\vec{x}_{(n \times 1)}$, respectively. In (1), $f(\vec{x}_{(n \times 1)})$ contains the integrand values evaluated at the nodes and it is a column vector with the same size as $\vec{x}_{(n \times 1)}$. This rule gives the exact integration results when the integrand $f(x)$ is at most an $(2n - 1)$th degree polynomial, and therefore it is called a $(2n - 1)$-degree quadrature rule. The n-point Gauss quadrature is one of the most efficient numerical integration schemes and it is widely used in the numerical analysis of different engineering problems. However, it cannot provide an error estimate of the numerical integration of arbitrary integrands in a single run, which can introduce problems when highly accurate results with fast computation times are needed. A solution to this problem was proposed by Alexander Kronrod [15]. He introduced $(n + 1)$ additional nodes (y_i) to the n-point Gauss quadrature rule to obtain the $(2n + 1)$-point Gauss-Kronrod rule as follows:

$$\int_a^b f(x)dx \approx K_{2n+1} = \sum_{i=1}^{n} \alpha_i f(x_i) + \sum_{j=1}^{n+1} \beta_j f(y_j) = \vec{\alpha} f(\vec{x}) + \vec{\beta} f(\vec{y}) \tag{2}$$

A comparison between (1) and (2) reveals that both integration rules use the same n nodes at $\vec{x}_{(n \times 1)}$. When constructing the Gauss-Kronrod rule in (2) the total number of $(3n + 2)$ unknowns introduced by the new weight and node vectors $\vec{\alpha}_{(1 \times n)}$ ($\vec{\alpha}_{(1 \times n)}$ is not same as $\vec{w}_{(1 \times n)}$), $\vec{\beta}_{(1 \times (n+1))}$ and $\vec{y}_{((n+1) \times 1)}$ values makes it possible to obtain a $(3n + 1)$-order quadrature rule [16]. In addition, a relative error estimate E of this rule can be readily obtained in a single run by comparing the result with n-point Gauss quadrature rule as follows:

$$E = \frac{|K_{2n+1} - G_n|}{|K_{2n+1}|} = \frac{|(\vec{\alpha} - \vec{w})f(\vec{x}) + \vec{\beta} f(\vec{y})|}{|\vec{\alpha} f(\vec{x}) + \vec{\beta} f(\vec{y})|} \tag{3}$$

In modern scientific computation software, such as Matlab [17,18], Octave [19] and quadpy [20], similar error estimates are used to build an adaptive Gauss-Kronrod integration scheme [21]. If an error criterion given by the user $E < \tau$ is not satisfied in an interval $[a, b]$, the Gauss-Kronrod rule is repeated on the sub-intervals $[a, (a + b)/2]$ and $[(a + b)/2, b]$. This division of intervals continues up until the error criteria is satisfied in all the sub-intervals. As a result, a robust numerical integration scheme is obtained that can be used efficiently in a variety of different engineering problems.

In some problem types, numerical integrations of similar integrands are needed. For example, when calculating the electromagnetic fields generated by a line source in planarly layered media by the Fourier type integrations, the same reflection and transmission coefficients are used to build up the spectral domain Green's functions. Since the results of the integrals, i.e., the spatial domain Green's functions, have the same type of plane wave constituents, the singularities, branch points and branch cuts are observed at the same locations in the spectral domain Green's functions defined for a given observation point. As a result, it is expected to have a similar, if not the same, distribution of nodes when performing the separate adaptive numerical integration of the Fourier type integrals by the Gauss-Kronrod quadrature rule as described above. By using this observation, the numerical integrations of different field components can be calculated simultaneously by using the same nodes (the same $\vec{x}_{(n \times 1)}$ and $\vec{y}_{((n+1) \times 1)}$ nodes in (2) are taken for different field components) along the same integration path. Consequently, the integrand is defined to be a row vector $\vec{f}_{(1 \times m)}(x)$ which contains the m similar integrand values at a given node x. If the node values are defined in a column vector as done in (1)-(3) $\vec{f}_{(1 \times m)}(\vec{x}_{(n \times 1)})$ becomes a matrix $\mathbf{F}_{(n \times m)}^x$, and likewise, $\vec{f}_{(1 \times m)}(\vec{y}_{((n+1) \times 1)})$ becomes a matrix $\mathbf{F}_{((n+1) \times m)}^y$. Therefore, the Gauss-Kronrod integration rule for the similar integrands can be written as follows:

$$\int_a^b \vec{f}(x)dx \approx \vec{K}_{2n+1} = \sum_{i=1}^{n} \alpha_i \vec{f}(x_i) + \sum_{j=1}^{n+1} \beta_j \vec{f}(y_j) = \vec{\alpha} \mathbf{F}^x + \vec{\beta} \mathbf{F}^y \tag{3}$$

In (4), $\vec{K}_{2n+1}$ is a $(1 \times m)$ row vector that contains the results of the $(2n+1)$ Gauss-Kronrod quadrature applied on the m similar integrands, $\vec{f}_{(1 \times m)}(x)$. As in the case of the single integrands, the adaptive integration scheme is applied as described until the error criteria is satisfied on all the sub-intervals, for all the integrands. It should be noted that for some integrands, this method will introduce more sub-intervals than necessary, but this will not affect the efficiency of the integration results and even lower numerical error values will be achieved for such integrands. Yet, an analysis would be needed to decide whether a simultaneous integration is needed or not depending on the constituents of the integrands. As discussed above, the calculation process of the fields generated by a line source in layered media is a case where the simultaneous numerical integration of the different field components would be used to obtain the results in a faster way compared to individual integrations. When using the simultaneous integration routine, the necessity of calculating the reflection and transmission coefficients separately for different field components is eliminated and the resulting numerical integrations are obtained within the same error criteria. The efficiency and the advantages of the method are demonstrated by numerical examples in the next section, both by analyzing general contour integrals with closed form results and the calculation performance of spatial domain Green's functions in layered media.

3.   Numerical Examples

In this section, the numerical integration scheme introduced in the previous section is validated by examples that are frequently seen in engineering applications. The performance of the new simultaneous integration algorithm is compared with the individual integration algorithm.

3.1.   Calculation of Contour Integrals with Analytical Results

In the first example, the integrals given in (5) with closed form analytical results found by the residue theorem [22] are numerically evaluated along the closed contour C shown in Figure 1. In (5), J_0 is the 0th order Bessel function of the first kind and $i = \sqrt{-1}$ is the unit complex number. In order to compare the performance of the different numerical integration routines analyzed in Chapter 2, the integrands are numerically integrated, first individually by the 15-point Gauss-Kronrod rule in (2) and then by the 15-point simultaneous integration rule derived in this paper in (4). For both integrations, the relative error stopping criteria are set to 10^{-10} and the initial number of nodes is set to 11, as it is done in most of the popular scientific software.

$$
\begin{aligned}
I_1 &= \oint_C \frac{J_0(2z)e^{i10z} - \cos(4z)}{(z - (0.5 - 0.1i))} \, dz \\[2mm]
I_2 &= \oint_C \frac{e^{i10z} - J_0(2z) + 2\cos(4z)}{(2z - (1 - 0.5i))(z - (0.5 - 0.1i))} \, dz \\[2mm]
I_3 &= \oint_C \frac{e^{i10z} - 3J_0(2z) + 2\cos(4z)}{(2z - (1 - 0.5i))(z - 0.33)(z - (0.5 - 0.1i))} \, dz \\[2mm]
I_4 &= \oint_C \frac{e^{i10z} + J_0(2z)\cos(4z)}{(z - 0.33)} \, dz
\end{aligned}
\tag{5}
$$

$$I_5 = \oint_C \frac{e^{i10z}0.5J_0(2z) + \cos(4z)}{(2z - (1 - 0.5i))}\,\mathrm{dz}$$

$$I_6 = \oint_C \frac{e^{i10z} + J_0(2z) + \cos(4z)}{(z - 0.33)(z - (0.5 - 0.1i))}\,\mathrm{dz}$$

$$I_7 = \oint_C \frac{J_0(2z)e^{i10z} + \cos(4z)}{(2z + (1 - 0.5i))(z + (0.5 - 0.1i))}\,\mathrm{dz}$$
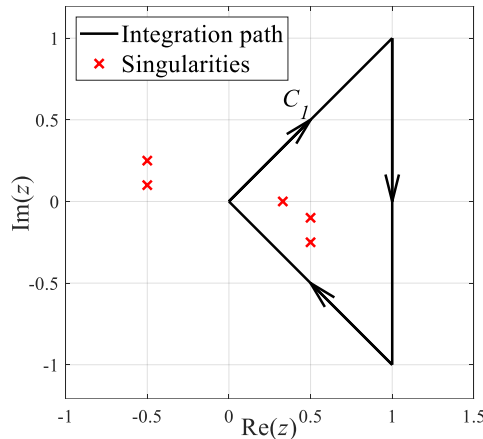

Figure 1. Integration path C used in (5) and the locations of the singularities of the integrands.

The results obtained by a single core of Intel(R) Xeon(R) CPU E5-2630 v3 using Matlab are shown in Table 1. As can be seen in the table, the relative errors compared with the analytical results are in the range of the stopping criteria for both integrations. The important difference is in the computation times, where an individual integration by (2) takes roughly 0.5ms and the simultaneous integration of all the integrands takes roughly 0.8ms. As a result, the total time for integrating all the 7 integrands is around 3.5ms which is around $\times 4.5$ slower than the simultaneous integration routine in (4). The main reason for this difference is eliminating the necessity of calculating the complex functions in the integrands repeatedly. When using the simultaneous integration routine, the functions are evaluated only once and used in all the integrands, since the same nodes are used in all the integrations. Whereas in the individual integration routine, a new set of nodes are used for all the different integrands.

Table 1. Numerical integration errors and computation times of the integrals in (5) obtained by the 15-point individual (2) and simultaneous (4) Gauss-Kronrod methods.

Integrand	Analytical result	Numerical Integration Error	Computation time (s)
I_1 (individual)	$-1.455734953472314e + 01$ $-8.014053318596627e + 00i$	$1.602939e - 13$ (relative)	$5.298821e - 04$
I_2 (individual)	$+4.744611107978165e + 01$ $-1.638584608339527e + 02i$	$6.943940e - 15$ (relative)	$5.425719e - 04$
I_3 (individual)	$+7.754555018569379e + 00$ $-1.126589747446449e + 02i$	$4.100069e - 15$ (relative)	$5.540496e - 04$
I_4 (individual)	$-9.911454277117049e - 01$ $+4.810429771194812e + 00i$	$2.705469e - 13$ (relative)	$5.326485e - 04$
I_5 (individual)	$-3.298687041869202e + 01$ $-1.010583291349705e + 01i$	$2.700818e - 14$ (relative)	$5.437397e - 04$
I_6 (individual)	$-3.940507818800279e + 01$ $-5.785451053909134e + 01i$	$2.548616e - 14$ (relative)	$5.418304e - 04$
I_7 (individual)	$+0 + 0i$	$5.006176e - 13$ (absolute)	$5.494489e - 04$
All (simultaneous)	Same as listed above	$4.963638e - 13$ (max)	$7.569228e - 04$

3.2. Calculation of Spatial Domain Green's functions by Sommerfeld Integrations

In the second example, the calculation performance of spatial domain Green's functions defined for a line source placed in a multilayered geometry is analyzed by using different numerical integration methods. As discussed earlier, to obtain the different components of electric and magnetic fields generated by a line source, separate Fourier type numerical integrations are needed. Yet, the singularities, branch points and cuts stay at the same locations on the integration plane for a given layered medium, which makes such problems good candidates for using the simultaneous integration routine introduced in this paper. By using the new simultaneous integration routine, it is expected to obtain the results of the Fourier-type integrals faster than the individual integrations without losing the precision of the results. In order to validate this expectation, the Green's functions of a 3-layered medium composed of left-handed (LHM), and right-handed (RHM) materials are calculated, first individually by the 15-point Gauss-Kronrod rule in (2) and then by the proposed 15-point simultaneous integration rule in (4). The specifications of the problem is as follows: the free-space wavelength of the source is 500nm, the layers are stacked from bottom to top and have the following electromagnetic properties: layer-1 (RHM, silver) $\varepsilon_{r1} = -9.621 + 0.31022i, \mu_{r1} = 1$, layer-2 (RHM, lossless) $\varepsilon_{r2} = 2, \mu_{r2} = 1$, and layer-3 (LHM, lossy) $\varepsilon_{r3} = -1 + 0.01i, \mu_{r3} = -1$. The thickness of the second layer is 500nm and layer 1 and 3 extend to infinity in y-direction. The magnetic-type line source is placed in the middle of layer-2. The magnitude of the Poynting vector $\vec{S}$ generated by the line source defined by:

$$\vec{S} = \vec{E} \times \vec{H}^*, \tag{6}$$

can be seen in Figure 2, for the 0 longitudinal dependence wave vector k_γ in (a) and $k_\gamma = (0.1 + 0.1i)k_0$ in (b), where k_0 is the wavenumber in free space. Since both the individual and simultaneous plots are identical, only the results of the simultaneous integration are plotted in the figure. The detailed derivations of the related integrands and integration paths are provided in [23–26].
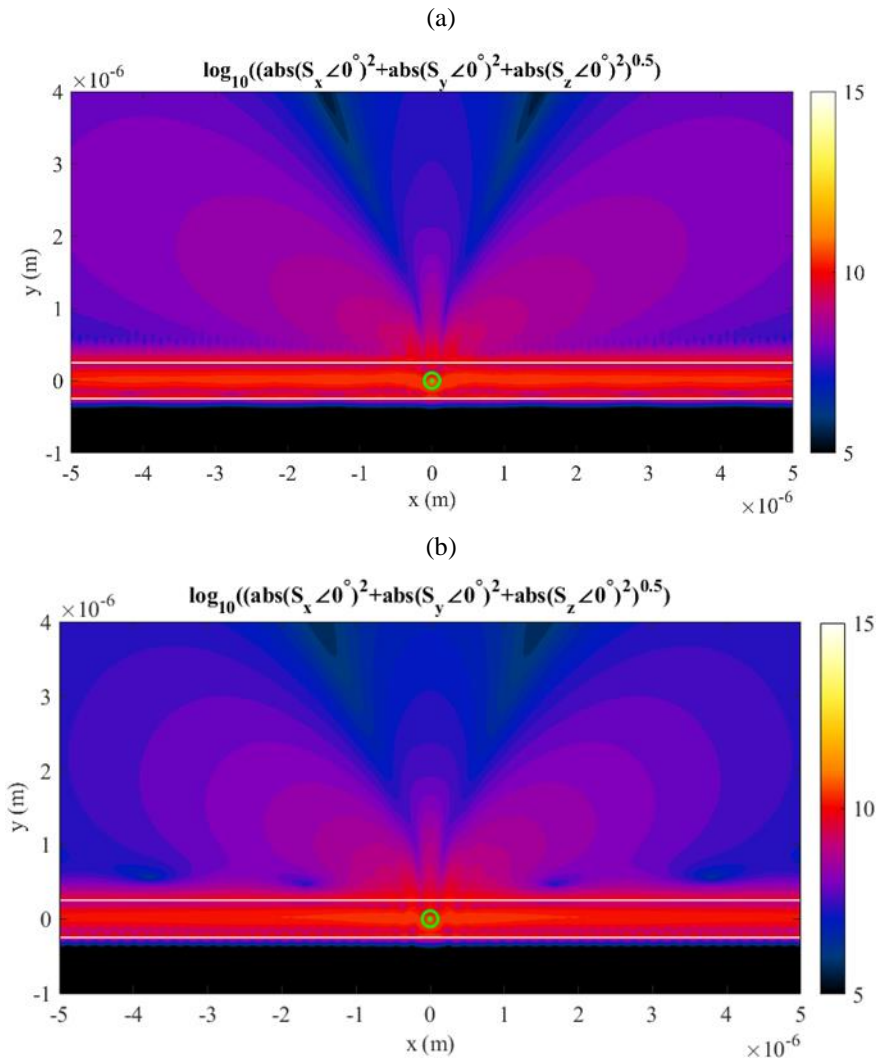
(a)

(b)

Figure 2. Magnitude of the Poynting vector in log scale generated by the magnetic line sources placed at the origin with the longitudinal dependence of (a): $k_\gamma = 0$ and (b): $k_\gamma = (0.1 + 0.1i)k_0$. Wavelength of the source is 500nm, layer-1 (bottom, RHM, silver) $\varepsilon_{r1} = -9.621 + 0.31022i, \mu_{r1} = 1$, layer-2 (RHM, lossless) $\varepsilon_{r2} = 2, \mu_{r2} = 1$, and layer-3 (LHM, lossy) $\varepsilon_{r3} = -1 + 0.01i, \mu_{r3} = -1$. The thickness of the second layer is 500nm.

As discussed earlier, the integrands derived for the electric and magnetic fields have similar shapes on the integration path and taking the simultaneous numerical integrals decreases the computation times significantly, which are compared in Table 2. The results in Figure 2 and Table 2 are obtained by 16 cores of Intel(R) Xeon(R) CPU E5-2630 v3 using Matlab. The field values are calculated on the grid defined by the 400 linearly spaced points in x-direction between -5 μm and 5 μm and the 200 linearly spaced points between -1 μm and 4 μm. Namely, the fields are calculated on the 80000 points on the field plane shown in Figure 2. The relative error stopping criteria of 10^{-6} is used in all the numerical integrations.

Table 2. Relative numerical integration errors and computation times of the Sommerfeld integrals when calculating the layered media Green's functions defined for the fields by the 15-point individual (2) and simultaneous (4) Gauss-Kronrod integrations.The calculated fields are used to plot Figure 2 by (6).

	Simultaneous $(k_\gamma = 0)$	Individual $(k_\gamma = 0)$	Simultaneous $(k_\gamma = (0.1 + 0.1i)k_0)$	Individual $(k_\gamma = (0.1 + 0.1i)k_0)$
Av. Error, E_x	$3.3622e - 09$	$2.0417e - 09$	$2.0417e - 09$	$2.3216e - 09$
Av. Error, E_y	$2.6046e - 09$	$1.9406e - 09$	$1.9406e - 09$	$1.9406e - 09$
Av. Error, E_z	N/A	N/A	$2.2708e - 12$	$1.1314e - 15$
Av. Error, H_x	N/A	N/A	$3.5034e - 09$	$3.5045e - 09$
Av. Error, H_y	N/A	N/A	$1.7555e - 07$	$1.8675e - 07$
Av. Error, H_z	$3.6108e - 09$	$3.6102e - 09$	$1.6110e - 09$	$1.6133e - 09$
Total time (s)	747	2135	1180	6817

Analyzing Table 2 reveals that, both integration methods give the results within the error criteria for the $k_\gamma = 0$ and $k_\gamma = (0.1 + 0.1i)k_0$ cases. The difference is observed in the calculation times, where the results are obtained nearly $\times 3$ times faster by the simultaneous integration routine when $k_\gamma = 0$ and nearly $\times 6$ faster when $k_\gamma = (0.1 + 0.1i)k_0$. This is the expected results as the magnetic line source generates 3 field components (E_x, E_y and H_z) when $k_\gamma = 0$ and it generates all the 6 field components when $k_\gamma \neq 0$. As a result of this comparison, it is shown that the simultaneous integration routine introduced in this paper can be used to obtain layered media Green's functions by the Sommerfeld integrations in a significantly faster way, without losing the accuracy of the results.

4. Conclusion

In this paper, a simultaneous numerical integration method is introduced. The main advantage of the proposed method is observed when a set of multiple integrations with similar integrands are needed. By using the method, the necessity of calculating the same functions repeatedly is eliminated and the integrands are obtained in a faster way. As a result, the integrals are calculated in a significantly faster way without decreasing the accuracy of the results. Examples are included to demonstrate the efficiency of the method by comparing the numerical integrations with analytical results and by analyzing the performance of the method when used in an advanced engineering problem.

References

[1]   Palacio-Betancur, A., & Gutierrez Soto, M. (2023). Recent Advances in Computational Methodologies for Real-Time Hybrid Simulation of Engineering Structures. *Archives of Computational Methods in Engineering*, *30*(3), 1637–1662. https://doi.org/10.1007/s11831-022-09848-y

[2]   Jiang, M., Li, Y., Lei, L., & Hu, J. (2022). A Review on Fast Direct Methods of Surface Integral Equations for Analysis of Electromagnetic Scattering from 3-D PEC Objects. *Electronics*, *11*(22), Article 22. https://doi.org/10.3390/electronics11223753

[3]   Botha, M. M. (2015). Numerical Integration Scheme for the Near-Singular Green Function Gradient on General Triangles. *IEEE Transactions on Antennas and Propagation*, *63*(10), 4435–4445. https://doi.org/10.1109/TAP.2015.2456959

[4]   Davis, P. J., & Rabinowitz, P. (2007). *Methods of Numerical Integration*. Courier Corporation.

[5] Kreyszig, E. (1999). *Advanced engineering mathematics* (8th ed). J. Wiley.

[6] Aimi, A., Diligenti, M., & Monegato, G. (1997). New Numerical Integration Schemes for Applications of Galerkin Bem to 2-D Problems. *International Journal for Numerical Methods in Engineering*, *40*(11), 1977–1999. https://doi.org/10.1002/(SICI)1097-0207(19970615)40:11<1977::AID-NME150>3.0.CO;2-O

[7] Felsen, N., & Marcuvitz, L. B. (1994). *Radiation and scattering of waves* (p. 924). John Wiley and Sons.

[8] Chew, W. C. (1990). *Waves and fields in inhomogeneous media*. New York: Van Nostrand Reinhold.

[9] Cheng, D. K. (1989). *Field and wave electromagnetics* (2nd ed.). Addison Wesley.

[10] Jin, J.-M. (2015). *The Finite Element Method in Electromagnetics*. John Wiley & Sons.

[11] Gibson, W. C. (2021). *The Method of Moments in Electromagnetics*. CRC Press.

[12] Harrington, R. F. (1982). *Field Computation by Moment Methods*. Florida: Robert E. Krieger Publishing Company.

[13] Hafner, C. (1999). *Post-Modern Electromagnetics: Using Intelligent Maxwell Solvers*. John Wiley and Sons.

[14] Kahaner, D., Moler, C., & Nash, S. (1989). *Numerical methods and software*. Prentice-Hall, Inc.

[15] Kronrod, A. S. (Aleksandr S. (1965). *Nodes and weights of quadrature formulas: Sixteen-place tables*. New York, Consultants Bureau. http://archive.org/details/nodesweightsofqu0000unse

[16] Laurie, D. (1997). Calculation of Gauss-Kronrod quadrature rules. *Mathematics of Computation*, *66*(219), 1133–1145. https://doi.org/10.1090/S0025-5718-97-00861-2

[17] *MATLAB - MathWorks—MATLAB & Simulink*. (n.d.). Retrieved February 1, 2023, from https://www.mathworks.com/products/matlab.html

[18] Shampine, L. F. (2008). Vectorized adaptive quadrature in MATLAB. *Journal of Computational and Applied Mathematics*, *211*(2), 131–140. https://doi.org/10.1016/j.cam.2006.11.021

[19] *GNU Octave*. (n.d.). Retrieved February 1, 2023, from https://octave.org/index

[20] Schlömer, N. (n.d.). *quadpy: Numerical integration, quadrature for various domains* (0.16.22) [Python; OS Independent]. Retrieved February 1, 2023, from https://github.com/sigma-py/quadpy

[21] Gonnet, P. (2012). A review of error estimation in adaptive quadrature. *ACM Computing Surveys*, *44*(4), 22:1-22:36. https://doi.org/10.1145/2333112.2333117

[22] Boas, M. (1983). *Mathematical methods in the physical sciences*. Wiley.

[23] Alparslan, A. (2023). Constituents of electromagnetic 2-D layered media Green's functions for all material types and radiation conditions. *Waves in Random and Complex Media*, 1–26. https://doi.org/10.1080/17455030.2023.2203264

[24] Michalski, K. A., & Mosig, J. R. (2015). The Sommerfeld half-space problem redux: Alternative field representations, role of Zenneck and surface plasmon waves. *IEEE Transactions on Antennas and Propagation*, *63*(12), 5777–5790. https://doi.org/10.1109/tap.2015.2489680

[25] Alparslan, A. (2013). *Numerical analysis of photonic nano structures in layered geometries* [ETH / ETH Zurich]. https://doi.org/10.3929/ethz-a-010000418

[26] Aksun, M. I. (1996). A robust approach for the derivation of closed-form Green's functions. *Microwave Theory and Techniques, IEEE Transactions On*, *44*(5), 651–658. https://doi.org/10.1109/22.493917